Supplementary Information

Pentacene and Tetracene Molecules and Films on H/Si(111): Level Alignment from Hybrid Density Functional Theory

Svenja M. Janke[1,2], Mariana Rossi[2,3], Sergey Levchenko[4,2], Sebastian Kokott[2], Matthias Scheffler[2] and Volker Blum[1,5]

[1] *Department of Mechanical Engineering and Materials Science, Duke University, Durham, NC, USA*
[2] *Fritz Haber Institute of the Max Planck Society, Berlin, Germany*
[3] *Max Planck Institute for the Structure and Dynamics of Matter, Hamburg, Germany*
[4] *Skolkovo Institute of Science and Technology, Moscow, Russia*
[5] *Department of Chemistry, Duke University, Durham, NC, USA*

The supplementary material contains the lattice parameters for bulk pentacene (Pc), tetracene (Tc) and Si; investigation of the validity of DFT-PBE+TS for structure relaxation for Film/ Substrate supercells; free-standing Tc and Pc monolayer lattice parameters and energies; H/Si(111) band gap convergence with slab thickness; check of non-interacting dilute limit for acene adsorption on H/Si(111); list of computational parameters for interface models; k-mesh test for interface models; overview over computational effort of the electronic structure calculations; free-standing monolayer relaxation geometries; numerical representation of films A-E for Pc and Tc on H/Si(111) supercells; lattice parameters and absorption energies for models of Pc and Tc on H/Si(111) interface models; definition of monolayer film adsorption distance; overview over frontier orbital energies in dilute and monolayer limit; the decomposition of the H/Si(111) surface density of states.

The electronic structure calculations that the work is based upon are available at the NOMAD CoE archive under DOI: https://dx.doi.org/10.17172/NOMAD/2020.06.23-1. Auxiliary output files are provided when they were used to derive the results presented in the paper.

Bulk Pentacene

Table S1: Comparison of the lattice parameters and angles of the crystal polymorph of pentacene obtained at 90 K and 300 K from x-ray diffraction [1] to values obtained after relaxation with DFT-PBE and Tkatchenko-Scheffler (TS) [2] as well as with many-body dispersion (MBD) [3] van der Waals (vdW) correction with "intermediate" settings within the FHI-aims code[4]. All atomic positions and lattice parameters were allowed to relax until residual forces on atoms and lattice vectors were below 0.005 eV/Å. The computational energy minimization of the structure used the lattice parameters and atomic positions as supplied in the T=90 K cif-file of the experimental publication [1] as its initial guess. The values obtained with DFT-PBE+TS are in good agreement with the DFT-PBE+MBD and experimental values.

	$\mathbf{a}_1$ (Å)	$\mathbf{a}_2$ (Å)	$\mathbf{c}$ (Å)	α (°)	β (°)	γ (°)
DFT-PBE+TS	6.13	7.62	14.53	78	87	85
DFT-PBE+MBD	6.28	7.68	14.35	76	89	84
90 K [1]	6.239(1)	7.636(1)	14.330 (2)	76.978(3)	88.136(3)	84.415(3)
300 K [1]	6.266(1)	7.775(1)	14.530(1)	76.475(4)	87.682(4)	84.684 (4)

Bulk Tetracene

Table S2: Comparison of the lattice parameters and angles of a tetracene crystal measured by x-ray diffraction [5, 6] to values obtained from geometry relaxation with DFT-PBE+TS and DFT-PBE+MBD at "intermediate" settings within the FHI-aims code[4]. All atomic positions and lattice parameters were allowed to relax until residual forces on atoms and lattice vectors were below 0.005 eV/Å. The relaxation used the lattice parameters and atomic positions as supplied in the cif-file of the experimental publication [5], CSD 114446 [7] as initial guess.

	$\mathbf{a}_1$ (Å)	$\mathbf{a}_2$ (Å)	$\mathbf{c}$ (Å)	α (°)	β (°)	γ (°)
DFT-PBE+TS	6.00	7.75	12.96	77	72	86
DFT-PBE+MBD	6.01	7.83	12.96	77	72	86
175 K [5]	6.0565(9)	7.8376(11)	13.0104(18)	77.127(2)	72.118(2)	85.792(2)
140 [6]	5.99(2)	7.77(4)	13.2(10)	102.4(5)	113.8(9)	86.0(4)
293 K [6]	6.065(2)	7.915(5)	13.445(12)	101.10(6)	113.31(9)	85.91(4)

Bulk Si

Table S3: Predicted lattice parameters for bulk Si using different density functionals and van der Waals corrections. Single point energy calculations for different unit cell volumes were performed using a $(12 \times 12 \times 12)$ k-point mesh and "tight settings" . The minimum-energy lattice parameters at the Born-Oppenheimer surface were then extracted by fitting total energies for the different volumes to the Birch-Murnaghan formula [8, 9].

Functional	a_0 (Å)
DFT-PBE	5.472
DFT-PBE+TS	5.450
DFT-PBE+MBD	5.436
HSE06+MBD	5.414
HSE06+TS	5.426
Lit. (RT) [10, 11]	5.431
Lit. (6.4 K) [12]	5.419

Investigation of Validity of PBE+TS for Structure Relaxation of Film/Substrate Supercells

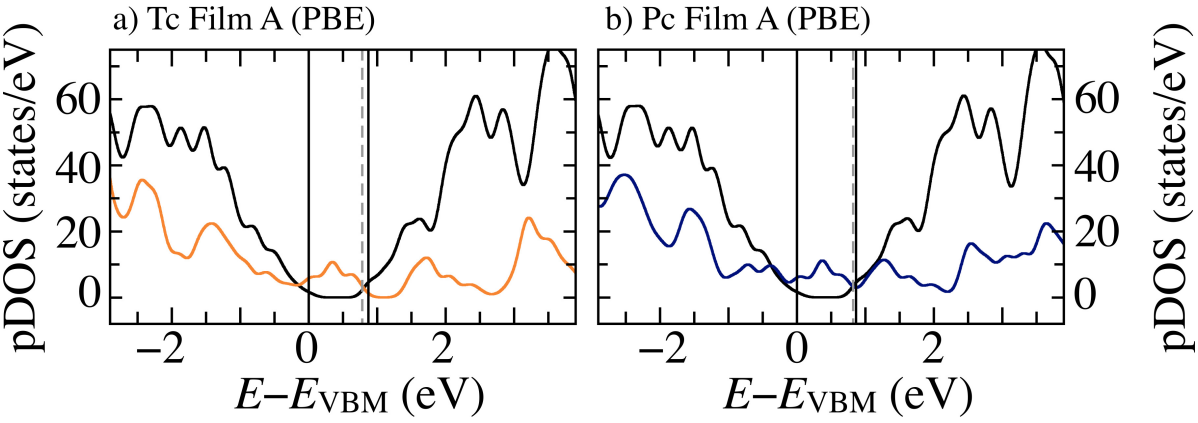

Figure S1: For Film A the PBE-calculated density of states projected onto the H/Si(111) surface atoms (black), a) onto the Tc film atoms (orange) and b) onto the Pc film atoms (blue) is shown. The positions of the inorganic VBM and CBM are marked by black lines and the position of the electronic chemical potential is marked as a dashed, grey line. It is well known that the electron delocalization error leads to a reduction of the band gap in semilocal functionals [13]. Given the small band gap observed with HSE06 hybrid functional for the film on substrate supercells in the main text but especially for Tc Film A and Pc Film B, the electronic delocalization error could hence lead to a closing of the band gap between the organic HOMO and the inorganic CBM when using the DFT-GGA functional PBE. Hypothetically, this would then allow charge redistribution from the acene films onto the H/Si(111). If charge were transferred, then the geometry of the film on the substrate could be substantially influenced. Then, PBE+TS would be unsuitable for structure optimization. To validate that structure optimization with PBE+TS is legitimate, we investigate orbital occupation for the Tc and Pc Film A supercells with Mulliken population analysis[14] on the PBE calculation. The results are shown in the pDOS above. For both Tc (a) and Pc (b) film A, the Fermi level is just below the inorganic CBM; the filled organic states avoid the empty inorganic states. Likewise, we performed a Hirshfeld analysis on partial charges on the atoms. Summation of the charges on film (Tc: −0.064 e; Pc: −0.045 e) and substrate (Tc: 0.065 e, Pc 0.043 e) shows negligible charging of film and substrate within the error margin of the method. We hence conclude that no erroneous charge transfer between the organic HOMO and inorganic CBM takes place for PBE+TS.

Free-Standing Monolayer Lattice Parameters and Energies

Table S4: In-plane lattice parameters of the Pc and Tc unit cells after relaxation, calculated using "intermediate" settings with DFT-PBE and TS [2] as well as with MBD [3] van der Waals (vdW) corrections and DFT-HSE06+TS [15–17]. All cells were rotated to have one of their lattice parameters parallel to the x-axis. Within the cells, all molecules assumed a herringbone pattern after relaxation. For Pc, unit cells were based on unit cell I determined for Pc dendrites on H/Si(111) [18]. For Tc, a unit cell was modeled with a herringbone pattern between two standing molecules based on the experimentally described geometry[19, 20]. For reference, relaxations for Tc were also performed based on the unit cell I used for Pc as a starting point. The resulting lattice vectors are almost identical. The energy is given with reference to the isolated molecule in vacuum as energy per molecule ΔE_{mol}. The two bottom lines show the lattice parameters from the experimental study of Pc dendrites on H/Si(111) at room temperature [18]. Their energy marked ([a]) corresponds to the energy after relaxation of the molecular positions with DFT-PBE+TS while the lattice parameters remained fixed to the experimental lattice parameters. The experimental error bars for the unit cell parameters are therefore included in the table and the notation "exp/PBE+TS" indicates the fact that experimental geometries (exp) and computed energies (DFT-PBE+TS) are combined in the lowest two lines.

	method	c_{11} (Å)	c_{12} (Å)	c_{21} (Å)	c_{22} (Å)	ΔE_{mol} (eV)
Pc (unit cell I based)	PBE+TS	5.85	0.00	0.00	7.36	**−1.974**
Tc (unit cell I based)	PBE+TS	5.83	0.00	0.02	7.41	**−1.556**
Tc (model)	PBE+TS	5.85	0.00	0.00	7.39	**−1.556**
Pc (unit cell I based)	PBE+MBD	5.89	0.00	0.00	7.40	**−1.588**
Tc (unit cell I based)	PBE+MBD	5.89	0.00	0.00	7.44	**−1.255**
Pc (unit cell I based)	HSE06+TS	5.77	0.00	0.00	7.32	**−2.204**
Tc (unit cell I based)	HSE06+TS	5.77	0.00	0.00	7.34	**−1.738**
Pc supercell I	exp/PBE+TS	6.02±0.01	0.00	0.00	7.62±0.01	−1.909[a]
Pc supercell II	exp/PBE+TS	5.98±0.01	0.00	0.00	7.56±0.01	−1.932[a]

H/Si(111) Band Gap Convergence with Slab Thickness

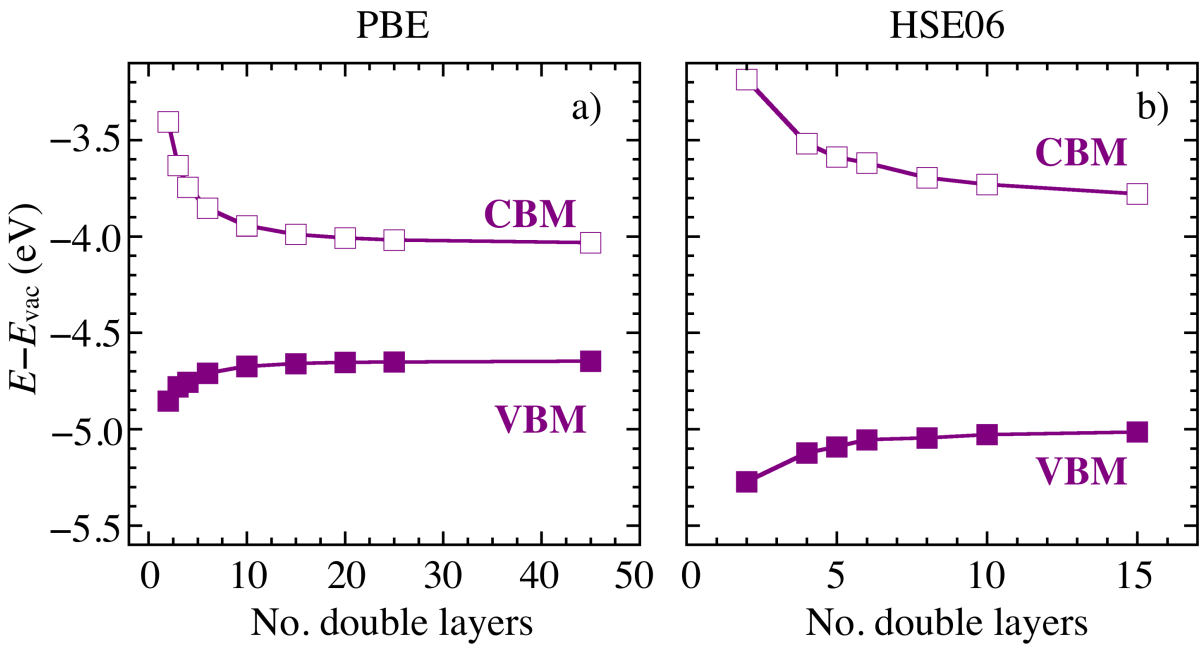

Figure S2: Variation of the valence band maximum (VBM, filled purple squares) and the conduction band minimum (CBM, open purple squares) of the H/Si(111) slab models as a function of the number of double layers. The energy axis values are referenced to the vacuum level ($E - E_{\mathrm{vac}}$). a) DFT-PBE results. b) DFT-HSE06 results from surfaces relaxed with DFT-PBE+TS and HSE06+TS. We relaxed $(1 \times 1 \times n)$ H/Si(111) slabs as a function of the number of Si double layers n in z-direction, using a $(12 \times 12 \times 1)$ k-point mesh and a vacuum layer thickness of 200 Å, until the minimum force was below 0.01 eV/Å with "tight" numerical settings of FHI-aims. The atomic positions of the top and bottom two Si double layers and the H atoms were relaxed while all others were kept fixed during the relaxation. The slow convergence of the band gap with the thickness of the slab has been observed previously for various Si surfaces [21–24] and is explained by a quantum well behavior due to confinement of the electronic eigenstates in thin slabs [23–25]. The DFT-HSE06 bulk band gap of 1.165 eV ("tight" settings) is close to the experimental value of 1.17 eV at T=0 K [11].

Dilute Limit of Acene Adsorption on H/Si(111)

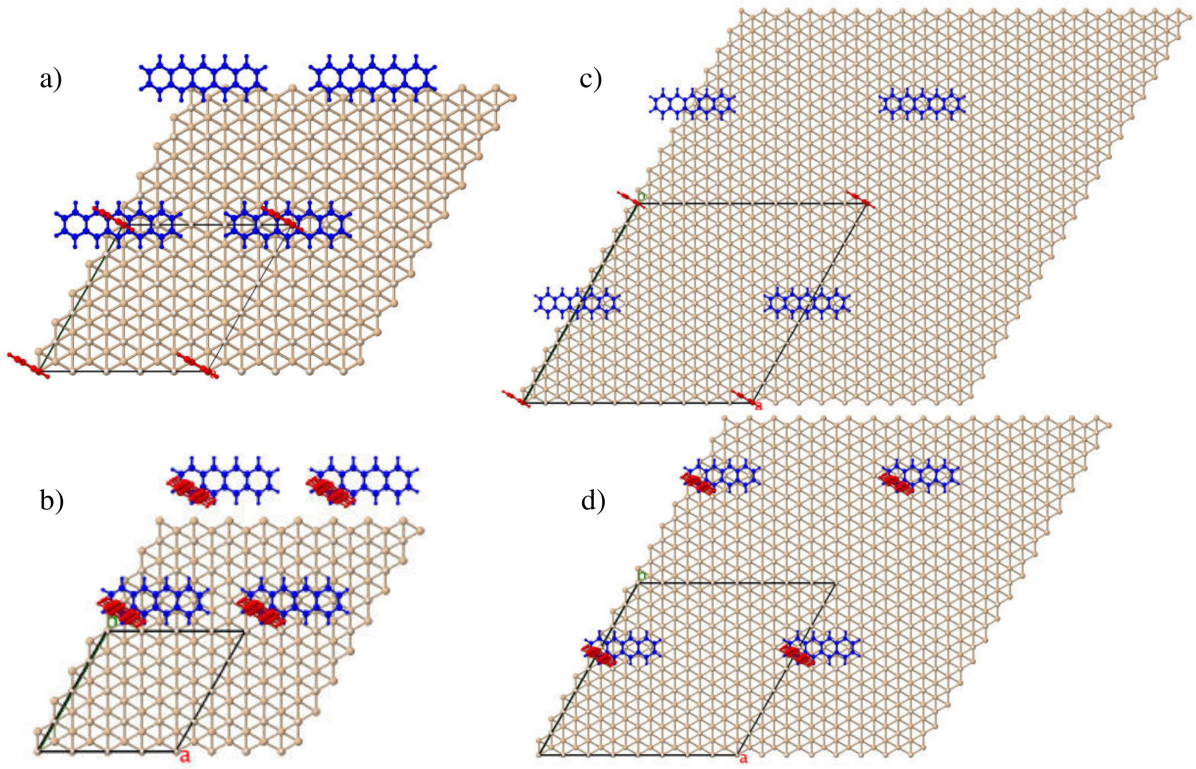

e)

Molecule	cell size	ΔE_{st} (eV)	ΔE_{ly} (eV)	$\Delta E_{\mathrm{st}} - \Delta E_{\mathrm{ly}}$ (eV)
Pc	5×5	-0.220	-1.420	-1.200
Pc	10×10	-0.234	-1.432	-1.198
Tc	4×4	-0.342	-1.186	-0.843
Tc	8×8	-0.347	-1.185	-0.838

Figure S3: Images of lying (blue) and standing (red) acenes adsorbed on H/Si(111) in the unit cells considered for the dilute limit in this work. We chose a cell size in xy-plane of (5×5) for Pc (a) and (4×4) for Tc (b) to isolate each molecule from its periodic images. If the cell size is doubled (c, d), the energy per molecule remains within a few meV of that of the smaller cell size (e, Table), both for a lying molecule (ΔE_{ly}) and a standing molecule (ΔE_{st}). Total energy calculations were performed using DFT-PBE+TS and "intermediate" settings. For the geometries in a–e, a previously relaxed $(1 \times 1 \times 10)$ double layer unit cell was repeated to form the different underlying slabs. For the positions of the molecules, we selected one molecule in a lying and one in a standing orientation from the structure search in Figure 3 of the main text. We then transferred the molecular positions to the slab models shown in this figure, keeping the distance to the average plane through the surface hydrogen atoms in the original structure.

Computational Parameters for Interface Models of the Dilute and Monolayer Limit

Table S5: For different models considered in the text, the table shows the unit cell area, total number of atoms (film and substrate) per unit cell, and k-point meshes used for structure relaxation (DFT-PBE+TS) and electronic structure calculation (HSE06). The HSE06 calculations were performed using the structures obtained with DFT-PBE+TS. "Intermediate" settings were used.

Model	area (Å^2)	No. Tc +H/Si(111) atoms per cell	No. Pc +H/Si(111) atoms per cell	DFT-PBE+TS k-point mesh	HSE06 k-point mesh
Dilute limit					
Pc	322		586	$(2 \times 2 \times 1)$	$(5 \times 5 \times 1)$
Tc	206	382		$(2 \times 2 \times 1)$	$(5 \times 5 \times 1)$
Monolayer limit					
A (Pc)			228	$(3 \times 5 \times 1)$	$(4 \times 7 \times 1)$
A (Tc)	77	204		$(4 \times 7 \times 1)$	$(4 \times 7 \times 1)$
B	347	858	954	$(6 \times 2 \times 1)$	$(3 \times 1 \times 1)$
C	424	1062	1182	$(6 \times 2 \times 1)$	$(1 \times 3 \times 1)$
D	309	756	840	$(6 \times 2 \times 1)$	$(3 \times 1 \times 1)$
E	424	1062	1182	$(6 \times 3 \times 1)$	$(4 \times 2 \times 1)$
Φ	283		740	$(6 \times 2 \times 1)$	$(6 \times 2 \times 1)$

K-mesh for Interface Models of the Dilute and Monolayer limit

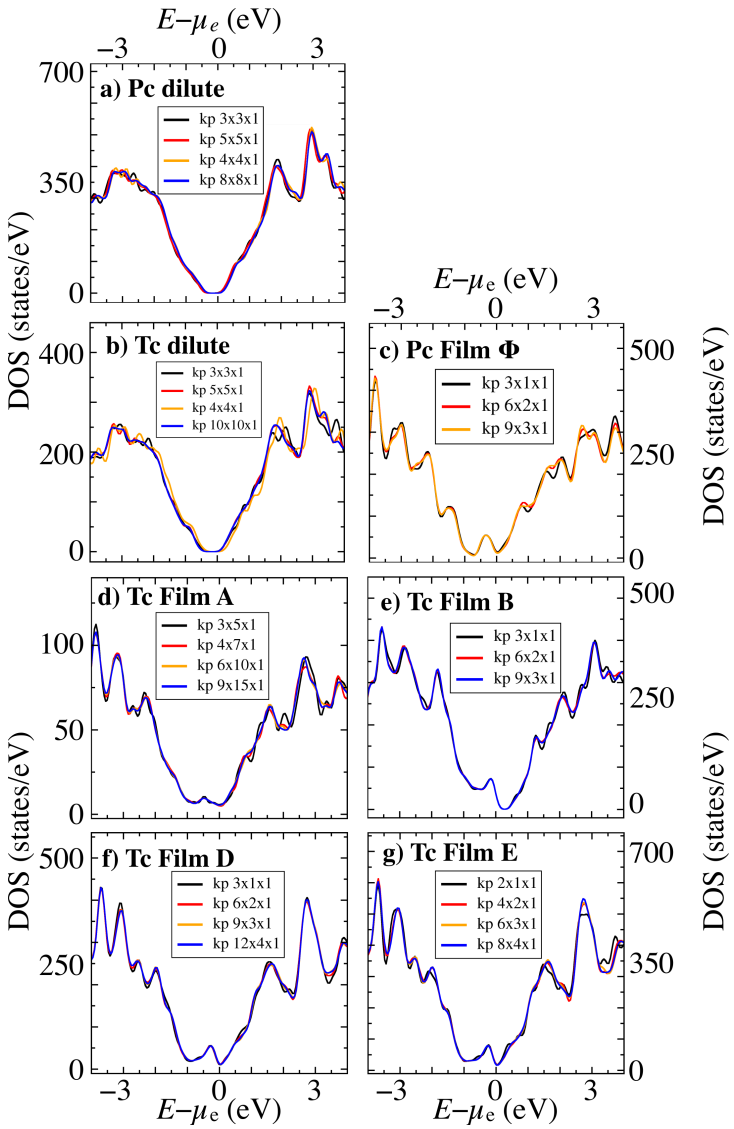

Figure S4: Comparison of total DOS for different k-point meshes for a) lying Pc, dilute limit; b) lying Tc, dilute limit; c) Pc Film Φ; d) Tc Film A; e) Tc film B; f) Tc film D; g) Tc Film E. The energy zero is set to the electronic chemical potential μ_e. The k-grids for the HSE06 calculations listed in Table S4 were chosen as the smallest possible ones to give a reasonable reproduction of the converged DOS. Note that Film C is not shown, because its $\mathbf{s}_1$ lattice parameter is identical to that of Film B and its $\mathbf{s}_2$ lattice parameter longer than that of Film B, so that if the k-grid for Film B is sufficient, the same k-grid will also be sufficient for Film C.

Computational Effort of Electronic Structure Calculations

Table S6: Overview over computational effort for the HSE06 level alignment calculations. To reduce the number of steps in the hybrid density functional theory calculations, the electronic density was (mostly) preconverged using the PBE functional. Calculations where then continued with the HSE06 functional using the preconverged density within the same overall calculation. The table gives an overview over the number of cores used in the calculations, the initialization time (init. time) and the average time per self-consistent cycle (time/SCF) as well as the number of steps in the calculation. In case HSE06 calculations had to be restarted to converged them, the density matrix of the final SCF step of the previous calculation was used. This is indicated by a sum of the number of SCF step. For cases were the number of cores was changed between the preconverging and final run, the HSE06 steps in the preconverging run are given in brackets. For the HSE06 calculations, timings are based on the final run. The calculations were performed on the COBRA supercomputer of the Max Planck Computing & Data Facility using Intel Xeon Gold 6148 Processors (Intel Skylake 6148) with 20 cores/node.

Limit	Model	PBE				HSE06			
		No. cores	t init. (s)	t/SCF (s)	No. steps	No. cores	t init. (s)	t/SCF (s)	No. steps
Tetracene Monolayer Limit	A	240	33.1	24.7	50	240	979	688	71
	B	1280	69.4	43.1	45	1280	2155	1800	40 + 3
	C					1920	2521	2264	7 + 12
	D	480	68.5	85.0	59	480	2764	2137	27 + 1
	E	1920	78.1	102.9	51	1920	2655	2574	27 + 1
Dilute Limit	Tc lying	240	126.7	149.7	39	240	3123	2748	17 + 2
	Tc standing	240	126.0	121.7	36	240	3155	2734	17 + 1
Pentacene Monolayer Limit	A	240	35.7	31.4	62	240	1282	881	77
	B	1920	45.9	38.9	55	1920	2140	1942	42 + 9
	C	1920	59.8	81.5	80	1920	2815	2584	9 + 16
	D	1280	50.8	43.8	56	1280	2003	1819	38 + 3
	E	1920	29.3	120.8	27	2564	3070	3138	(16) + 11
	Φ	480	122.0	129.9	46	1280	2000	1949	(0) + 14
Dilute Limit	Pc lying	240	264.1	281.6	38	480	4327	4281	(0) + 13
	Pc standing	480	228.0	248.7	50	640	4077	4204	(15)+3

Free-Standing Monolayer Relaxation Geometries

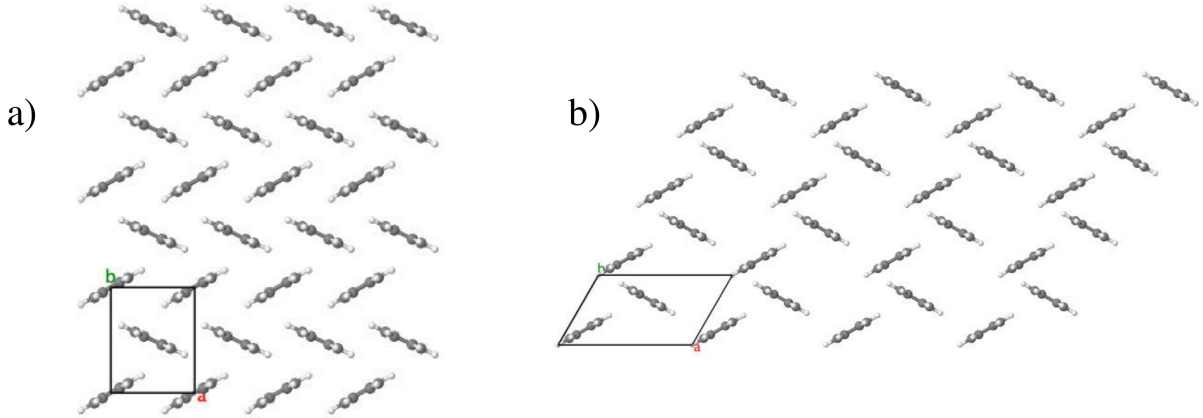

Figure S5: Initial geometry before relaxation of a Pc (a) and Tc (b) monolayer in vacuum viewed along **c**-direction. The unit cell used in the relaxation is indicated by a black frame. For Pc, the initial unit cell was based on the unit cell I structure suggested by Nishikata *et al.* [18]. For Tc, the initial unit cell was based on the observation that Tc molecules assume a standing orientation and a herringbone pattern on weakly interacting surfaces [19]. Relaxations were performed with PBE+TS and "intermediate" settings until all residual forces on atoms and lattice vectors were below 0.005 eV/Å.

Numerical Representation of for Films A–E for Pc on H/Si(111) Supercells

Table S7: Numerical representation of the strained film supercells (SCs) A–E at the example of Pc from Figure 6a) – c) according to Eq.s (2), (3) and (4) of the main text. The matrix of the in-(001)-plane lattice vectors of the combined film-substrate supercell **S** is a multiple (**C**) of the substrate lattice vectors $\mathbf{b}_1$ and $\mathbf{b}_2$ (see Eq.(2)). The strain transformation of the supercell parameters of the film **F** when the film is combined with the substrate is expressed in terms of the matrix **T** (Eq. (4)). $|\mathbf{T}|$ describes the agreement between the area of the substrate and monolayer film supercell.

Film	α (°)	**S** (Å)		**C**		$\mathbf{T}_{\mathrm{Pc}}$		$\lvert\mathbf{T}\rvert_{\mathrm{Pc}}$
A	0	11.561	0.000	3	3	0.988	0.000	0.895
		0.000	6.675	−1	1	0.000	0.906	
B	0	11.561	0.000	3	3	0.988	0.000	1.007
		5.781	30.037	−3	6	−0.016	1.020	
C	0	11.561	0.000	3	3	0.988	0.000	0.985
		5.781	36.712	−4	7	−0.005	0.997	
D	315	13.488	−3.337	4	3	1.022	−0.012	1.023
		25.049	16.687	4	9	0.004	1.001	
E	300	5.781	−10.012	3	0	0.988	0.000	0.985
		34.684	13.350	7	11	−0.005	0.997	

Numerical Representation of for Films A–E for Tc on H/Si(111) Supercells

Table S8: Numerical representation of the strained film supercells (SCs) A–E at the example of Pc from Figure 6a) – c) according to Eq.s (2), (3) and (4) of the main text. The matrix of the in-(001)-plane lattice vectors of the combined film-substrate supercell **S** is a multiple (**C**) of the substrate lattice vectors $\mathbf{a}_1$ and $\mathbf{a}_2$ (see Eq.(3)). The strain transformation of the supercell parameters of the film **F** when the film is combined with the substrate is expressed in terms of the matrix **T** (Eq. (4)). $|\mathbf{T}|$ describes the agreement between the area of the substrate and monolayer film supercell. The values in $\mathbf{T}_{\mathrm{Tc}}$ and $|\mathbf{T}|_{\mathrm{Tc}}$ are almost identical to those for Pc in Tab. S8, due to the similarity of the lattice parameters between Tc and Pc.

Film	α (°)	**S** (Å)		**C**		$\mathbf{T}_{\mathrm{Tc}}$		$\lvert\mathbf{T}\rvert_{\mathrm{Tc}}$
A	0	11.561	0.000	3	3	0.976	0.000	0.889
		0.000	6.675	−1	1	0.000	0.910	
B	0	11.561	0.000	3	3	0.976	0.000	1.000
		5.781	30.037	−3	6	−0.024	1.024	
C	0	11.561	0.000	3	3	0.976	0.000	0.977
		5.781	36.712	−4	7	−0.013	1.001	
D	315	13.488	−3.337	4	3	1.008	−0.007	1.016
		25.049	16.687	4	9	−0.005	1.007	
E	300	5.781	−10.012	3	0	0.976	0.000	0.977
		34.684	13.350	7	11	−0.013	1.001	

Models of Monolayer Pentacene Interfaces with H/Si(111): Geometries and Energies

Table S9: For pentacene, the lattice parameters and angle γ between the lattice vectors, the energy per molecule ΔE, the average angle θ of the molecules to the surface normal, the average herringbone angle ω and the average distance d_z of the z-component of the molecules' center of mass to the plane through the average height of the first layer of Si atoms (see Figure S4) are shown.

Film	**a** (Å)	**b** (Å)	$\gamma(^\circ)$	ΔE (eV)	θ ($^\circ$)	ω ($^\circ$)	d_z (Å)
free-standing	5.85	7.36	90				
A	5.78	6.68	90	−2.022	1	46	10.0
B	5.78	30.59	79	−2.213	1	54	10.2
C	5.78	37.16	81	−2.221	1	52	10.1
D	13.90	30.10	48	−2.175	1	51	10.2
E	5.78	37.16	81	−2.221	1	52	10.1
Φ	6.13	7.71	87	−2.222	22	49	9.5

Models of Monolayer Tetracene Interfaces with H/Si(111): Geometries and Energies

Table S10: For tetracene, the lattice parameters and angle γ between the lattice vectors, the energy per molecule ΔE, the average angle θ of the molecules to the surface normal, the average herringbone angle ω and the average distance d_z of the z-component of the molecules' center of mass to the plane through the average height of the first layer of Si atoms (see Figure S6) are shown.

Film	**a** (Å)	**b** (Å)	$\gamma(^\circ)$	ΔE (eV)	θ ($^\circ$)	ω ($^\circ$)	d_z (Å)
free-standing	5.85	7.39	90				
A	5.78	6.68	90	−1.625	1	46	8.8
B	5.78	30.59	79	−1.798	1	54	8.9
C	5.78	37.16	81	−1.762	1	53	8.9
D	13.90	30.10	48	−1.780	8	51	8.9
E	5.78	37.16	81	−1.802	1	53	8.9

Definition of Monolayer Film Adsorption Distance

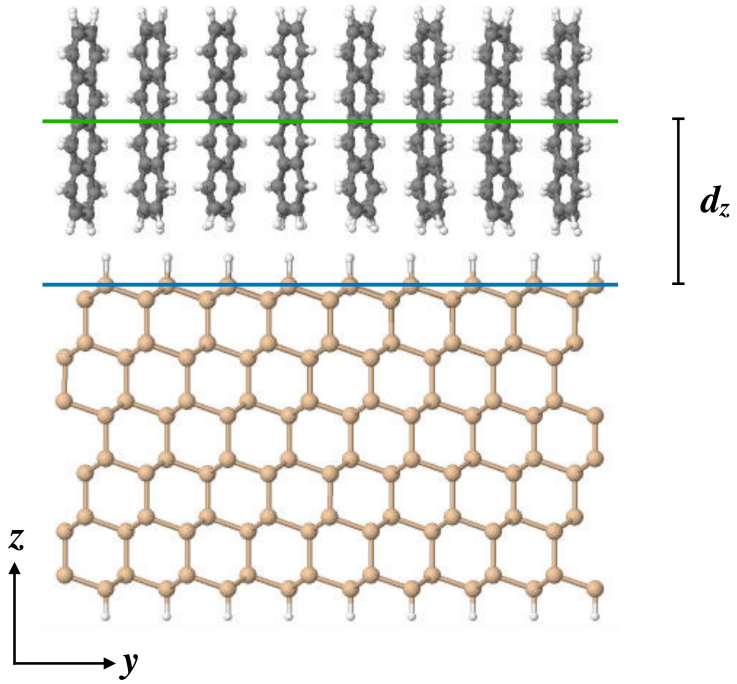

Figure S6: Side view of the slab model of a tetracene film on H/Si(111), model B. The adsorption distance d_z of a molecule to the substrate is defined as the distance between the z-component of the center-of-mass of the molecular atoms (green line) and the plane defined by the average z-position of the top layer of Si atoms (blue line).

Frontier Orbital Energies in the Dilute and Monolayer Limits

Table S11: The DFT-HSE06 energy and the gaps of the VBM and CBM of the substrate and HOMO and LUMO of the film extracted from HSE06 Mulliken analysis, counting all contributions above 0.0025 total occupation. The band gap of the isolated substrate (PBE+TS geometry, calculated with HSE06, "intermediate" settings) is 1.465 eV, the gaps given for "Tetracene" and "Pentacene" correspond to those of the isolated molecule in vacuum.

Limit	Model	substrate			film			overall
		VBM (eV)	CBM (eV)	gap (eV)	HOMO (eV)	LUMO (eV)	gap (eV)	band gap (eV)
Isolated	Tetracene						2.269	
Monolayer Limit	A	-5.59	-4.08	1.51	-4.41	-3.31	1.10	0.33
	B	-5.53	-4.07	1.46	-4.86	-3.03	1.83	0.79
	C	-5.54	-4.07	1.47	-4.76	-3.07	1.68	0.69
	D	-5.52	-4.02	1.50	-4.78	-3.07	1.71	0.76
	E	-5.54	-4.07	1.47	-4.80	-3.06	1.74	0.73
Dilute Limit	Tc lying	-5.40	-4.07	1.33	-5.68	-3.51	2.17	1.61
	Tc standing	-5.42	-4.08	1.33	-5.42	-3.21	2.21	1.33
Isolated	Pentacene						1.696	
Monolayer Limit	A	-5.67	-4.16	-1.50	-4.30	-3.86	-0.44	0.14
	B	-5.59	-4.13	1.46	-4.58	-3.42	1.16	0.45
	C	-5.60	-4.13	1.47	-4.53	-3.44	1.09	0.40
	D	-5.66	-4.16	1.50	-4.66	-3.52	1.14	0.50
	E	-5.61	-4.14	1.46	-4.53	-3.44	1.09	0.39
	Φ	-5.53	-4.06	1.46	-4.64	-3.59	1.05	0.58
Dilute Limit	Pc lying	-5.40	-4.07	1.33	-5.38	-3.74	1.63	1.31
	Pc standing	-5.42	-4.09	1.33	-5.14	-3.45	1.69	1.06

H/Si(111) Surface Density of States Decomposition

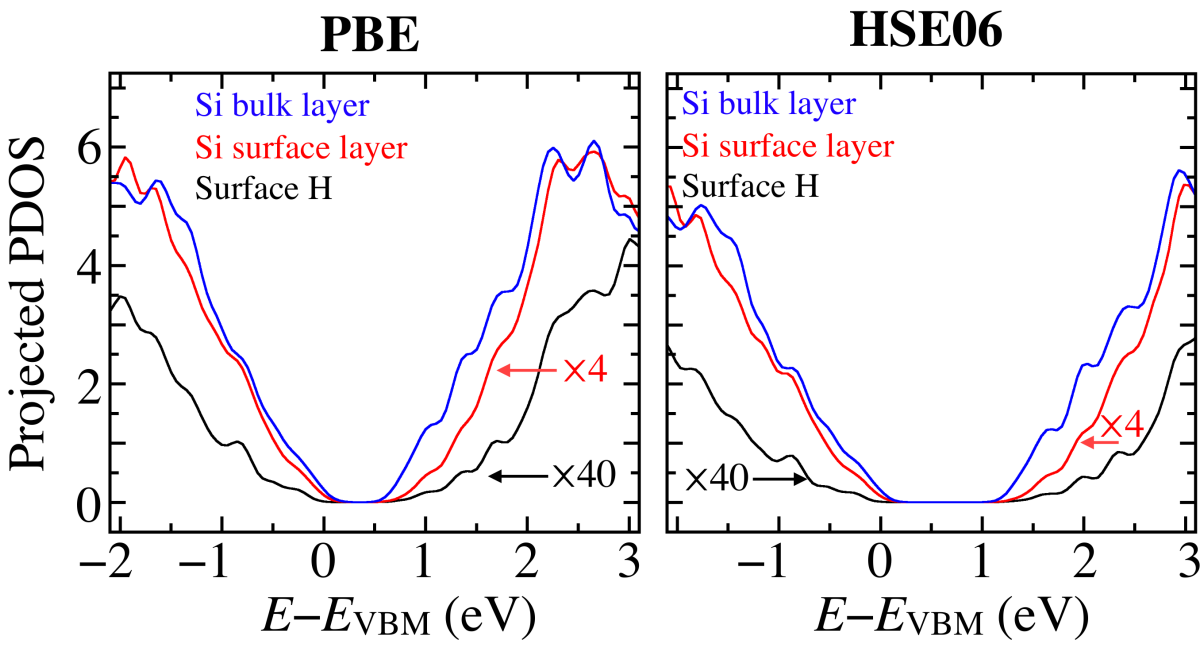

Figure S7: Projected densities of states onto surface H (black), Si bulk layers (blue) and Si surface layers (red) for 10 Si double layers in H/Si(111) calculated with PBE (left) and HSE06 (right) from surfaces relaxed with DFT-PBE+TS and HSE06+TS at "intermediate" settings of FHI-aims. The curves of the surface H and surface Si are scaled by a factor of 40 and 4, respectively. The onset of the band gap is formed by contributions from the bulk layers (blue).

References

[1] C. C. Mattheus, A. B. Dros, J. Baas, A. Meetsma, J. L. d. Boer, and T. T. M. Palstra, "Polymorphism in pentacene," *Acta Crystallographica Section C*, vol. 57, no. 8, pp. 939–941, 2001.

[2] A. Tkatchenko and M. Scheffler, "Accurate molecular van der waals interactions from ground-state electron density and free-atom reference data," *Physical Review Letters*, vol. 102, p. 073005, 2009.

[3] A. Ambrosetti, A. M. Reilly, R. A. D. Jr., and A. Tkatchenko, "Long-range correlation energy calculated from coupled atomic response functions," *The Journal of Chemical Physics*, vol. 140, no. 18, p. 18A508, 2014.

[4] V. Blum, R. Gehrke, F. Hanke, P. Havu, V. Havu, X. Ren, K. Reuter, and M. Scheffler, "Ab initio molecular simulations with numeric atom-centered orbitals," *Computer Physics Communications*, vol. 180, no. 11, pp. 2175–2196, 2009.

[5] D. Holmes, S. Kumaraswamy, A. J. Matzger, and K. P. C. Vollhardt, "On the nature of nonplanarity in the [n]phenylenes," *Chemistry – A European Journal*, vol. 5, no. 11, pp. 3399–3412, 1999.

[6] U. Sondermann, A. Kutoglu, and H. Bassler, "X-ray diffraction study of the phase transition in crystalline tetracene," *The Journal of Physical Chemistry*, vol. 89, no. 9, pp. 1735–1741, 1985.

[7] C. R. Groom, I. J. Bruno, M. P. Lightfoot, and S. C. Ward, "The Cambridge Structural Database," *Acta Crystallographica Section B*, vol. 72, no. 2, pp. 171–179, 2016.

[8] F. D. Murnaghan, "The compressibility of media under extreme pressures," *Proceedings of the National Academy of Sciences*, vol. 30, no. 9, pp. 244–247, 1944.

[9] F. Birch, "Finite elastic strain of cubic crystals," *Physical Review*, vol. 71, pp. 809–824, 1947.

[10] CRC Handbook of Chemistry and Physics, Internet Version, 2005. p.9–44.

[11] C. Kittel, *Introduction to Solid State Physics*. John Wiley & Sons, 2005.

[12] D. N. Batchelder and R. O. Simmons, "Lattice constants and thermal expansivities of silicon and of calcium fluoride between 6 and 322 k," *The Journal of Chemical Physics*, vol. 41, no. 8, pp. 2324–2329, 1964.

[13] G. Onida, L. Reining, and A. Rubio, "Electronic excitations: density-functional versus many-body green's-function approaches," *Rev. Mod. Phys.*, vol. 74, pp. 601–659, Jun 2002.

[14] R. S. Mulliken, "Electronic population analysis on lcao-mo molecular wave functions. i," *The Journal of Chemical Physics*, vol. 23, no. 10, pp. 1833–1840, 1955.

[15] J. Heyd, G. E. Scuseria, and M. Ernzerhof, "Hybrid functionals based on a screened coulomb potential," *The Journal of Chemical Physics*, vol. 118, no. 18, pp. 8207–8215, 2003.

[16] J. Heyd, G. E. Scuseria, and M. Ernzerhof, "Erratum: Hybrid functionals based on a screened coulomb potential [j. chem. phys. 118, 8207 (2003)]," *The Journal of Chemical Physics*, vol. 124, no. 21, p. 219906, 2006.

[17] A. V. Krukau, O. A. Vydrov, A. F. Izmaylov, and G. E. Scuseria, "Influence of the exchange screening parameter on the performance of screened hybrid functionals," *The Journal of Chemical Physics*, vol. 125, no. 22, 2006.

[18] S. Nishikata, G. Sazaki, J. T. Sadowski, A. Al-Mahboob, T. Nishihara, Y. Fujikawa, S. Suto, T. Sakurai, and K. Nakajima, "Polycrystalline domain structure of pentacene thin films epitaxially grown on a hydrogen-terminated si(111) surface," *Physical Review B*, vol. 76, p. 165424, 2007.

[19] J. Shi and X. R. Qin, "Flux dependence of the morphology of a tetracene film on hydrogen-passivated si(100)," *Physical Review B*, vol. 73, p. 121303, 2006.

[20] A. Tersigni, J. Shi, D. T. Jiang, and X. R. Qin, "Structure of tetracene films on hydrogen-passivated si(001) studied via stm, afm, and nexafs," *Physical Review B*, vol. 74, p. 205326, 2006.

[21] Y. Li and G. Galli, "Electronic and spectroscopic properties of the hydrogen-terminated si(111) surface from ab initio calculations," *Physical Review B*, vol. 82, p. 045321, 2010.

[22] K. Sagisaka, J. Nara, and D. Bowler, "Importance of bulk states for the electronic structure of semiconductor surfaces: implications for finite slabs," *Journal of Physics: Condensed Matter*, vol. 29, no. 14, p. 145502, 2017.

[23] B. Delley and E. F. Steigmeier, "Size dependence of band gaps in silicon nanostructures," *Applied Physics Letters*, vol. 67, no. 16, pp. 2370–2372, 1995.

[24] P. Scherpelz and G. Galli, "Optimizing surface defects for atomic-scale electronics: Si dangling bonds," *Physical Review Materials*, vol. 1, p. 021602, 2017.

[25] M. V. Fischetti, B. Fu, S. Narayanan, and J. Kim, *Semiclassical and Quantum Electronic Transport in Nanometer-Scale Structures: Empirical Pseudopotential Band Structure, Monte Carlo Simulations and Pauli Master Equation*, pp. 183–247. New York, NY: Springer New York, 2011.